Observation of local-interfacial optical phonons at buried interfaces using time-resolved second-harmonic generation

Y.-M. Chang, L. Xu, and H. W. K. Tom
Department of Physics, University of California, Riverside, California 92521
(Received 5 January 1999)

We have used an all-optical technique to observe optical phonons localized at a buried interface. The technique is based on coherent excitation of the interfacial vibrational mode by femtosecond laser irradiation and detection of the free-induction decay of the coherent oscillation by time-resolved second-harmonic generation. For native oxide-covered GaAs (100), we observe a single-optical phonon mode at 8.48 ± 0.04 THz localized to a few monolayers on the semiconductor side of the interface. The assignment is based on changes in the phonon spectrum as a function of pump-laser intensity and during *in situ* oxidation. The mode frequency shifts from 8.48 to 8.29 THz due to coupling with holes driven to the interface by the depletion field.
[S0163-1829(99)00619-0]

Despite the importance of understanding and controlling the structure and electronic properties of interfaces between dense media (buried interfaces), few experimental probes are sensitive to the local properties of the few monolayers of atoms arranged differently at the interface than they are arranged in the bulk. Vibrational (phonon) spectroscopy provides an important microscopic probe of structure, bonding, and dynamics. Coherent studies of surface acoustic-wave velocities have been reported,[1] however, optical phonons in the range 3–10 THz are more sensitive to local (atomic-scale) geometry because these modes involve counter-propagating atomic motion analogous to vibrational modes in molecules. Optical techniques such as Fourier transform infrared (IR) spectroscopy, free-electron laser-based IR spectroscopy, and visible-IR sum-frequency generation and Raman spectroscopy have been developed and demonstrated for adsorbate molecules at vacuum and gas/solid interfaces. In principle, extension to buried interfaces is straightforward if at least one side of the interface is optically transparent. However, IR phonon or plasmon absorption in the surrounding bulk media prevents all but Raman from being generally applicable to buried interfaces. Raman spectroscopy is used to measure high-frequency vibrational modes of adsorbate molecules at liquid/solid interfaces and bulklike phonon features at buried interfaces. Despite the almost routine application of Raman, only one case of monolayer-scale local phonons at buried interfaces has been reported: spontaneous Raman[2] and resonance Raman spectroscopy of Sb monolayers on GaAs.[3] Helium atom scattering and high-resolution electron-energy-loss spectroscopy (HREELS) in the impact regime have submonolayer sensitivity to surface adsorbates. In the long-range dipole interaction regime, HREELS has been used to observe Fuchs-Kliewer (F-K) phonons at clean[4] and buried semiconductor interfaces,[5,6] and bulklike modes[6] and standing wave modes[7] in thin-film overlayers. While F-K phonons and thin-film layer modes are confined to the interfacial region and may be sensitive to monolayer-scale interfacial properties through the induced interface current,[6] the phonon displacements are dominated by bulk properties and are not ''localized'' to the monolayer scale structure at the interface.

In an earlier paper we introduced a technique for studying optical phonons on surfaces prepared in ultrahigh vacuum (UHV) by time-resolved surface second-harmonic generation.[8] Here we demonstrate that the technique is sensitive enough to observe a local optical-phonon mode at a buried interface. We observe a mode localized to a few (1–4) monolayers of the GaAs (100) native-oxide interface. Previous Raman studies of this interface have only been able to detect lines for bulk GaAs LO and TO phonons and bulk of As crystallites that form in thick oxides,[9] and numerous other studies suggest that Raman scattering does not generally have the sensitivity to detect local-interfacial phonon modes. The significance of this paper is that this technique may have the sensitivity to open the door to atomic-scale investigation of a wide variety of buried interfaces.

Pump and probe beam were derived from the output of a Kerr-lens modelocked Ti:Sapphire laser oscillator operating at 850 nm with 30 fs pulse duration and 80 MHz repetition rate. The probe beam was time delayed with respect to the pump with an optical delay line. The two parallel beams were focused using a 5 cm focal-length plano-convex singlet lens to overlap on the sample with $\sim 3°$ angular separation. The beams were incident at $\sim 45°$ angle of incidence and the sample was held in air or in a UHV chamber. The *p*-polarized second-harmonic generation (SHG) of the *p*-polarized probe beam was detected as a function of pump-probe time delay. The SH was separated from the fundamental with color and interference filters and detected with a cooled photomultiplier tube. The pump-induced change in the probe SH was obtained with a lock-in amplifier synchronized to a mechanical chopper that chopped the pump beam. The pump-probe cross-correlation SH signal on sample was used to establish the zero of time delay. The probe intensity was less than the pump and we verified that the probe intensity did not influence the results. The range of time delay was scanned every few minutes and 20 to 100 scans were averaged.

The GaAs (100) sample was highly *n*-doped (3×10^{18} Si/cm^3) and the depletion field was calculated to be 740 kV/cm over the topmost 140 Å. The native oxide is ~ 50–80 Å thick. The clean GaAs (100) 4×6 surface was

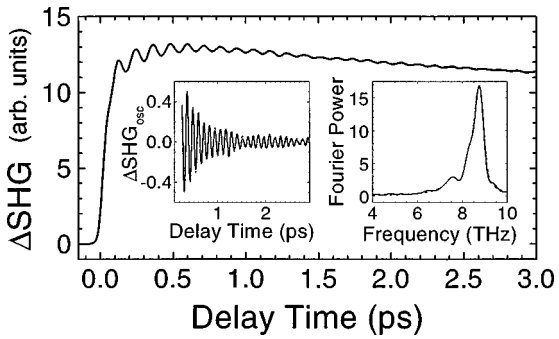

FIG. 1. TRSHG signal for native-oxide-covered GaAs (100). The injected carrier density was $7.2\times10^{17}/\mathrm{cm}^3$. Left and right insets show the oscillatory part of the time-domain data and the apodized Fourier power spectrum of the oscillatory part. Data (solid) and fit (dashed).

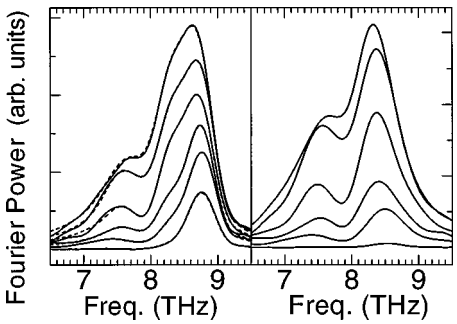

FIG. 2. (Left) Fourier power spectra of the TRSHG of native-oxide-covered GaAs (100). From smallest to largest amplitude curve, peak injected carrier densities were 1.2, 4.8, 7.2, 11, 15, and 22 ($\times10^{17}/\mathrm{cm}^3$). (Right) Fourier power spectrum of $S_{\mathrm{OSC}}(t)$ data minus the free-induction decay of the 8.80 THz mode obtained by fit.

prepared in UHV by cycles of 400 eV Ar^+ ion sputtering and thermal annealing at 550 °C for 30 min until Auger electron spectroscopy showed <1% oxygen (our limit) and low-energy electron diffraction (LEED) showed a sharp pattern [without $c(8\times2)$ features]. The SH measures the nonlinear optical response at the buried interface and in the topmost 200 Å of the GaAs bulk. The probe depth is determined by optical-phase matching and the optical penetration depth (which is short for the SH frequency). SH is always dipole allowed at interfaces. SH from bulk GaAs has two sources: DC field-induced SH in the depletion region and dipole-allowed bulk SH, which can be rejected by choice of crystal orientation.[10]

In Fig. 1 we show the time-resolved pump-induced change in SHG (TRSHG) from the GaAs (100)—native-oxide interface held in air. We see a rapid change near zero time delay due to carrier injection and rapid carrier-induced screening of the depletion field. A slow (~10 ps) decay follows as the depletion field recovers by carrier diffusion and recombination dynamics. Ultrafast carrier dynamics in the depletion region is well studied and is known to drive coherent LO phonon oscillations in the bulk.[11] We focus presently on the small oscillation on this background signal. Because this data is obtained over many scans the oscillation is coherent with the arrival of the pump pulse and due to excitation of coherent optical phonons.

The SH intensity vs time delay is proportional to the square of the SH susceptibility, which we may separate into a transient background and oscillatory part. Both the oscillation amplitude and slow transient decay are ~10% of the pump-induced TRSHG signal and only ~1% of the total probe SHG intensity. We obtain a signal (left inset) proportional to the oscillatory part $S_{\mathrm{OSC}}(t)$ by simply cutting off the first 150 fs of delay time and subtracting the transient background. The latter is obtained by Fourier smoothing out frequencies >3 THz. This procedure produces cross-term artifacts between the transient background and oscillations of order 0.01% that we can neglect.

After the initial excitation, each phonon mode follows damped harmonic motion. We therefore fit $S_{\mathrm{OSC}}(t) = \Sigma_n A_n e^{-t/T_n}\cos(2\pi f_n t+\varphi_n)$, where T_n, f_n, and φ_n are the dephasing time, resonant frequency, and initial phase of the nth mode, respectively. The coefficients A_n are proportional to the product of the peak displacement amplitude of the nth mode and the hyper-Raman tensor $\partial\chi^{(2)}(2\omega)/\partial\hat{Q}_n\cdot\hat{Q}_n$ is the displacement unit vector of the nth mode. Our experiments are the coherent time-domain analog of stimulated hyper-Raman spectroscopy. We obtain the frequency spectrum by Fourier transform. For an infinite time interval the Fourier transform is the sum of complex Lorentzians. We suppress the artifacts introduced into the spectrum by the finite time interval of the data by using an apodizing function of the form $\sin[\alpha(t-t')]/[\alpha(t-t')]$ with width chosen to minimally impact the phonon features. When we fit the data (dashed lines in all figures), we iteratively compare the time-domain and apodized complex Fourier transform of the data with the fit function over the same time interval. The apodized power spectrum (right inset) is the square of the apodized complex Fourier transform.

In Fig. 2 (left), the apodized power spectra of $S_{\mathrm{OSC}}(t)$ data for the native-oxide-covered GaAs (100) are shown for various injected carrier densities (i.e., pump fluence). The photoinjected carrier density at the sample surface is calculated using the literature values of the optical constants[12] integrated over the measured frequency spectrum of our femtosecond laser pulse. We fit the data to three modes (i.e., 12 unknowns). The highest-frequency mode stays fixed at 8.80 ±0.015 THz, the middle-frequency mode shifts from 8.48 to 8.29 THz, and the lowest-frequency mode shifts monotonically from 7.52 to 7.67 THz. The error bar is ±0.04 THz in these fits due to nonlinear coupling with the other parameters. In coherent time-domain spectroscopy, the power spectrum is the square of the sum (not the sum of the squares) of complex Lorentzians. Lineshapes can be complicated by superposition of dispersive and absorptive features of neighboring lines. To better visualize the validity of the fit, in Fig. 2 (right) we plot the power spectra of the $S_{\mathrm{OSC}}(t)$ data minus the free-induction decay of the 8.80 THz mode obtained by fitting. The ~8.4 THz mode is clearly observed as well as the lack of the remaining 8.80 THz mode susceptibility.

The 8.80 THz mode is the well-known bulk LO phonon mode at $q=0$. The depletion field creates a static LO phonon displacement near the surface by the piezoelectric effect. Injected carriers rapidly screen the depletion field and permit the lattice to freely oscillate about the field-free equilibrium positions. At low injected carrier density the LO phonon motion has a frequency of 8.80 THz because carriers are swept

out of the depletion region. At higher injected carrier density, the plasma modes of the carriers remaining in the depletion region couple to the LO phonon motion. The observed 7.5–7.67 THz mode is consistent with the frequency, frequency shift, and dephasing time of the LO phonon-electron plasmon coupled mode. As more electrons are injected the frequency shifts toward the bulk TO phonon frequency 8.0 THz. Both modes are well understood physically and their coherent excitation has been studied by Kurz and co-workers[11,13] using time-resolved linear-reflectivity measurements.

The mode at ~8.4 THz is a local interfacial mode confined to a few monolayers of the interface. The data in Fig. 2 allow us to argue that it cannot be anything else. It cannot be a pure bulk mode. Our excitation region is the 140-Å deep depletion region over the ~20 μm laser-spot diameter. Expansion of this motion as a superposition of pure bulk modes can only involve modes with $q_{\|} < (1\,\mu\mathrm{m})^{-1}$ and $q_z < (200\,\text{Å})^{-1}$ for which there is a gap between the bulk TO and LO phonon frequencies at 8.0 and 8.8 THz. The ~8.4 THz mode cannot be the bulk LO phonon-electron plasmon coupled mode, which is observed at frequencies <8.0 THz. It cannot be the LO phonon-hole plasmon coupled mode. The topmost 25 Å of the interface is hole-rich due to the separation of the photoinjected carriers in the depletion region. Raman studies in *p*-doped GaAs show the bulk LO phonon-hole plasmon coupled-mode frequency shifts continuously from the LO frequency to the TO frequency as a function of hole density.[14] However, we do not detect phonon motion at frequencies between 8.8 and 8.5 THz as a function of injected carrier density. Second, at our highest-injected carrier density we expect the hole density to be $>10^{19}/\mathrm{cm}^3$ (using a numerical simulation following Ref. 13), and the coupled mode to shift to 8.0 THz. For a frequency of ~8.4 THz, the expected dephasing time for the coupled mode would be 180 fs, which is 2.5 times lower than the measured value.

The ~8.4 THz mode cannot be a Fuchs-Kliewer mode. The F-K mode is a phonon mode coupled to the field induced by the interfacial charge oscillation that the phonon itself creates at the dielectric discontinuity of the interface. The F-K modes have a bulk LO phononlike lattice displacement that is elliptically polarized and varies sinusoidally along the surface and exponentially into the bulk as $\exp(iq_{\|}x - q_{\|}z)$.[15] The relation between bulk LO and F-K modes is analogous to the relation between bulk plasmons and interface plasmons. Indeed, for semiconductors, the F-K mode is often strongly coupled to interface plasmon modes.[4] HREELS detects these modes efficiently. However, we do not expect to excite or detect these modes efficiently. In the TRSHG case, both the driving force and probe are applied to a relatively shallow (140–200 Å) and wide (20-μm in diameter) region, and thus will have poor spatial overlap with any of the F-K modes. Second, if the ~8.4 THz mode was spatially extended over depths greater than the depletion region, we would expect to see it in time-resolved linear-reflection measurements. We have not observed this mode nor have Kurz and co-workers.

Now we argue that the ~8.4 THz mode must be spatially localized to a few atomic layers of the interface because it is sensitive to changes in the first monolayer of oxide. In Fig. 3

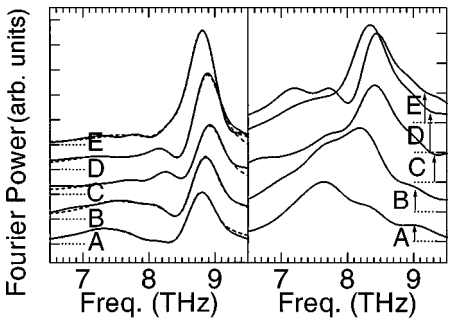

FIG. 3. Fourier power spectra of $S_{\mathrm{OSC}}(t)$ data (left) and $S_{\mathrm{OSC}}(t)$ data minus the fitted free-induction decay of the 8.80 THz mode (right) from clean GaAs (100)-4×6 vs O_2 exposures (Langmuir): (a) clean surface, (b) 10^2 L, (c) 10^4 L, and (d) 10^6 L, (e) native-oxide-covered surface in UHV chamber. The injected carrier density was $1.8\times10^{17}/\mathrm{cm}^3$. Data (solid) and fit (dashed). Curves are offset vertically by tick mark units.

(left), we show the apodized power spectra of the $S_{\mathrm{OSC}}(t)$ data from the GaAs (100)-(4×6) at various stages of *in situ* oxidation. The fluence is fixed so we ignore fluence dependence and the intensity is low enough to ignore the LO phonon-electron plasmon coupled mode compared to clean-surface phonon modes. The native-oxide data (curve E) was measured in the UHV chamber with nominally identical laser conditions as for curves A–D but before the oxide was removed and the surface was cleaned. Oxygen was backfilled into the chamber in the presence of a lit nude ion-gauge filament. Adsorption of O atoms produced by cracking molecular O_2 at the hot filament is known to proceed efficiently. In this geometry, our SHG studies show oxidation of dangling bonds proceeds with Langmuir kinetics at the rate of $(1200\,\mathrm{L})^{-1}$. The apparent shift of the 8.8 THz feature to higher frequency in C-D is due to mixing with a weak mode at ~9.3 THz, which we will not discuss further.

In Fig. 3 (right), we show the power spectra of the $S_{\mathrm{OSC}}(t)$ data minus the free-induction decay of the LO phonon obtained by fitting [as we did in Fig. 2(b)]. The progression from curve A to D clearly establishes the monolayer sensitivity of this technique and is consistent with all modes in curve A other than the 8.8 THz mode being localized to 1–3 monolayers of the reconstructed surface. The sequence from A to C clearly shows the growth of a narrow mode peak ~8.4 THz. The near absence of the mode in curve A shows that this is not a bulk phonon-hole plasmon coupled mode or F-K mode. The ~8.4 THz mode amplitude and linewidth do not substantially change from C to D and to E (the native-oxide-covered surface) suggesting that the physical structure that vibrates is already established once the dangling bonds are oxidized. To be so sensitive to adsorbed oxygen, the mode displacement must be dominated by motion only a few atomic bond lengths away from the oxide.

The most likely assignment of the mode is to an oxidation strain-induced interface mode localized in the topmost 2–3 atomic layers of the semiconductor. In *ab initio* calculations of the phonon spectra of clean GaAs (110), modes between 8.0 and 8.8 THz are associated with in-plane Ga-As counterpropagating motion dominated by motion in the second and third layers.[16] Hydrogenation completely relaxes the dangling bond-induced strain in the reconstructed layer.[17] How-

ever, it is likely that the larger size and strength of the Ga-O bond as well as steric effects associated with the larger oxygen atom strain the underlying semiconductor layers. Curves C and D are consistent with the mode frequency being stable almost as soon as the strain of the first oxide monolayer is established. Such an assignment is consistent with sensitivity to submonolayer oxygen adsorption. The oxide is known to be atomically abrupt but disordered. Additional amorphous oxide layers would not be expected to substantially change the interfacial strain. The similarity between D and E suggests that even when oxygen penetrates the bulk and forms disordered gallium oxide, the bonding geometry at the interface is controlled by the local geometry of the Ga-O bond and is thus similar to that produced by a single monolayer of adsorbed oxide.

The 8.48 THz mode frequency shifts to 8.29 THz as a function of injected carrier density. The interface mode-center frequencies obtained by fit in Fig. 2 are 8.48, 8.45, 8.34, 8.28, 8.36, and 8.29 THz respectively, with error bars ± 0.04 THz. A downward shift in phonon frequency is consistent with coupling to hole plasmons because the holes are overdamped. In simulations following Ref. 11, the maximum surface-hole density is $10^{19}/\mathrm{cm}^3$, at which density the hole plasma should fully screen the polarization induced by the phonon itself and 8.29 THz would be the intrinsic (transverse-optical) mode frequency. Because this mode is confined spatially on a monolayer scale, however, the bulk dielectric analysis is probably not applicable and further analysis including the high-hole density and the induced-interface charge oscillation is necessary. The observed dephasing times range from 700 to 430 fs and are 2–3 times longer than one would expect for bulk modes coupled to the overdamped hole plasma using the bulk dielectric analysis.

It is unlikely that the 8.48 THz mode is due to Ga-O or As-O vibrational modes. The relatively large signal size is not consistent with the smaller polarizability one would expect for tightly bound Ga-O. The linewidths are also not consistent with the inhomogeneous broadening expected between B and E for this atomically disordered oxide. For completeness, we mention that spectral changes could be partially caused by changes in the Raman or hyper-Raman susceptibilities due to changes in the oxidation-induced electronic structure. Electronic resonance at the Sb/GaAs interface enhances the Raman susceptibility of the interface phonon modes.[3] The E_2 state induced by strain at the SiO_2/Si interface enhances SH.[18] This caveat does not contradict the assignment of the mode as an interfacial one confined to a few monolayers, which is based on both eliminating other possible assignments (Fig. 2) and showing the right characteristics for a local mode (Fig. 3).

In closing, the ability to characterize monolayer scale structure and study carrier-phonon interaction at buried interfaces is an essentially unexplored area of interface science. We have shown that a new time-domain analog of coherent hyper-Raman spectroscopy has adequate sensitivity to measure local phonon spectra at a buried interface. With signal-to-noise improvements, this technique may be useful for studying local phonon modes at a variety of buried interfaces.

The authors gratefully acknowledge support under NSF Grant No. CHE-9707143.

[1] C. Thompsen, H. T. Grahn, H. J. Maris, and J. Tauc, Phys. Rev. B **34**, 4129 (1986); O. B. Wright and K. Kawashima, Phys. Rev. Lett. **69**, 1668 (1992).

[2] M. Hunermann, J. Geurts, and W. Richter, Phys. Rev. Lett. **66**, 640 (1991).

[3] N. Esser, M. Kopp, P. Haier, A. Kelnberger, and W. Richter, J. Vac. Sci. Technol. B **11**, 1481 (1993).

[4] R. Matz and H. Lüth, Phys. Rev. Lett. **46**, 500 (1981); L. H. Dubois and G. P. Schwartz, Phys. Rev. B **26**, 794 (1982).

[5] Ph. Lambin *et al.*, Phys. Rev. Lett. **56**, 1842 (1986).

[6] M. Liehr, P. A. Thiry, J. J. Pireaux, and R. Caudano, Phys. Rev. B **34**, 7471 (1986).

[7] P. Senet, Ph. Lambin, and A. A. Lucas, Phys. Rev. Lett. **74**, 570 (1995).

[8] Y. M. Chang, L. Xu, and H. W. K. Tom, Phys. Rev. Lett. **78**, 4649 (1997).

[9] N. Levinson *et al.*, Appl. Phys. Lett. **56**, 1131 (1990); A. Rim and R. Beserman, J. Appl. Phys. **74**, 897 (1993).

[10] T. Stehlin, M. Feller, P. Guyot-Sionnest, and Y. R. Shen, Opt. Lett. **13**, 389 (1988).

[11] W. A. Kütt, W. Albrecht, and H. Kurz, IEEE J. Quantum Electron. **28**, 2434 (1992).

[12] C. H. Kuo *et al.*, J. Vac. Sci. Technol. B **12**, 1214 (1994).

[13] G. C. Cho *et al.*, Phys. Rev. Lett. **77**, 4062 (1996).

[14] K. Wan and J. F. Young, Phys. Rev. B **41**, 10 772 (1990).

[15] R. Fuchs and K. L. Kliewer, Phys. Rev. **140**, 2076 (1965).

[16] J. Fritsch, P. Pavone, and U. Schröder, Phys. Rev. Lett. **71**, 4194 (1993).

[17] J. Fritsch, A. Eckert, P. Pavone, and U. Schröder, J. Phys.: Condens. Matter **7**, 7717 (1995).

[18] W. Daum, H.-J. Krause, U. Reichel, and H. Ibach, Phys. Rev. Lett. **71**, 1234 (1993); C. Meyer *et al.*, *ibid.* **74**, 3001 (1995).